VIP Modified Graphitic Networks Very Important Paper

DOI: 10.1002/ange.201310260

Direct Solvothermal Synthesis of B/N-Doped Graphene**

*Sun-Min Jung, Eun Kwang Lee, Min Choi, Dongbin Shin, In-Yup Jeon, Jeong-Min Seo, Hu Young Jeong, Noejung Park, Joon Hak Oh, and Jong-Beom Baek**

Abstract: *Heteroatom-doping into graphitic networks has been utilized for opening the band gap of graphene. However, boron-doping into the graphitic framework is extremely limited, whereas nitrogen-doping is relatively feasible. Herein, boron/nitrogen co-doped graphene (BCN-graphene) is directly synthesized from the reaction of CCl_4, BBr_3, and N_2 in the presence of potassium. The resultant BCN-graphene has boron and nitrogen contents of 2.38 and 2.66 atom %, respectively, and displays good dispersion stability in N-methyl-2-pyrrolidone, allowing for solution casting fabrication of a field-effect transistor. The device displays an on/off ratio of 10.7 with an optical band gap of 3.3 eV. Considering the scalability of the production method and the benefits of solution processability, BCN-graphene has high potential for many practical applications.*

Since the early experimental studies on graphene in 2004,[1] it has been the focus of vigorous application research owing to its outstanding properties, including high specific surface area,[2] good thermal and electrical conductivity,[3,4] and superior optical properties,[5] among others.[6,7] However, in order to take advantage of the outstanding properties of graphene in practice, the development of feasible synthetic methods and chemical modifications to provide multifunctionality and processability for specific applications becomes an important challenge. For example, chemical and/or physical doping, such as covalently doping heteroatoms into the graphitic structure,[8] and the physisorption of gases,[9] metals,[10,11] or organic molecules[12] on the surface of graphene, are useful for enhancing the electrocatalytic activity of solar[13] and fuel cells,[14] as well as controlling the band-gap state.[15] However, the covalent introduction of heteroatoms into the graphitic framework is not enough to tune the properties of graphene.[16]

Graphene is a semimetal with no band gap.[17] As a result, it is not suitable for logic applications, because devices cannot be switched off. Therefore, graphene must be modified if it is to be used in electronic devices. Various methods of making graphene-based field-effect transistors (FETs) have been researched, including doping graphene,[18] tailoring a graphene like nanoribbon,[19] and by using boron nitride as a support.[20] Among the methods of controlling the band gap of graphene, doping methods show the most industrial feasibility. By co-doping boron and nitrogen into carbon nanotubes and graphene[21] using a chemical vapor deposition (CVD) process, semiconducting behavior was achieved.[22,23] It is believed that doping graphene through a solvothermal method would produce similar semiconducting behavior.

Herein, we report an efficient method for the mass production of boron/nitrogen co-doped graphene (BCN-graphene) nanoplatelets by the solvothermal reaction of carbon tetrachloride (CCl_4) and potassium (K) in the presence of boron tribromide (BBr_3) and nitrogen (N_2). Notably, whereas this method is extremely limited for B-doping into the graphitic framework using BBr_3 by itself,[24] it is feasible for boron/nitrogen co-doping in the presence of BBr_3 together with nitrogen. The resultant BCN-graphene nanoplatelets displayed an on/off current ratio of ca. 10.7 in a FET device.

In order to optimize the reaction conditions and provide a baseline for later comparison, carbon-based graphene (C-graphene) was prepared by the solvothermal Wurtz reaction.[24–26] In brief, the reaction between alkyl halides (e.g. CCl_4) and alkaline metals (e.g. potassium) generates carbon radicals and precipitated alkaline metal halides (e.g. potassium chloride; Figure 1a). The carbon radicals then form carbon–carbon (C–C) bonds on the surface of the alkaline metal particles. The fast radical reaction is spontaneously driven by high thermodynamic energy gain (formation energy plus crystal lattice energy) from K–K and 2 C–Cl bonds to 2 KCl and a C–C bond (Figure 1a, inset). The product (C-graphene) has a dark black color, indicating the formation of a graphitic structure, along with white KCl crystals deposited on the reactor wall (Figure 1a, photograph). The optimized reaction conditions for C-graphene were used for the synthesis of boron-doped graphene (BC-graphene) by adding BBr_3 under an argon atmosphere or for boron/nitrogen-doped graphene (BCN-graphene) by adding BBr_3 under a nitrogen atmosphere. The key difference in the reaction

[*] S.-M. Jung, M. Choi, D. Shin, I.-Y. Jeon, J.-M. Seo, Prof. N. Park, Prof. J.-B. Baek
Interdisciplinary School of Green Energy/Low-Dimensional Carbon Materials Center, Ulsan National Institute of Science and Technology (UNIST), Ulsan, 689-798 (South Korea)
E-mail: jbbaek@unist.ac.kr
Homepage: http://jbbaek.unist.ac.kr
E. K. Lee, Prof. J. H. Oh
School of Energy and Chemical Engineering/Low-Dimensional Carbon Materials Center, Ulsan National Institute of Science and Technology (UNIST), Ulsan, 689-798 (South Korea)
Prof. H. Y. Jeong
UNIST Central Research Facilities/School of Mechanical & Advanced Materials Engineering, Ulsan National Institute of Science and Technology (UNIST), Ulsan, 689-798 (South Korea)

[**] This research was supported by Mid-Career Researcher (MCR), BK21 Plus, Basic Science Research (BSR), Converging Research Center (CRC), and Basic Research Laboratory (BRL) programs funded by the National Research Foundation (NRF) of Korea, and the US Air Force Office of Scientific Research through the Asian Office of Aerospace R&D (AFOSR-AOARD). E.K.L. would like to acknowledge a Global Ph.D. Fellowship.

Supporting information for this article is available on the WWW under http://dx.doi.org/10.1002/anie.201310260.

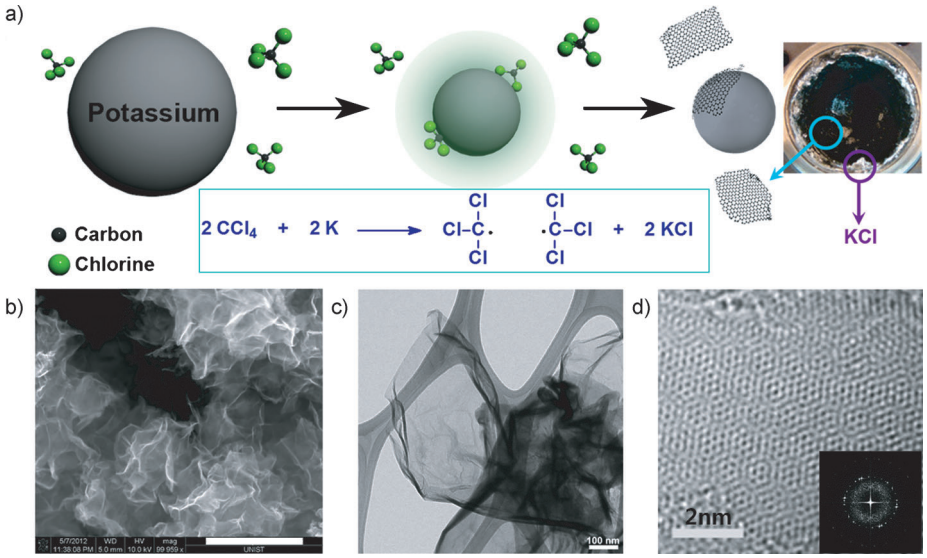

Figure 1. a) The formation of C-graphene by solvothermal reaction between carbon tetrachloride (CCl_4) and potassium. Photograph is of the autoclave after the reaction, showing the formation of C-graphene (black) and potassium chloride (KCl; white). b) SEM image of BCN-graphene. Scale bar is 1 μm. c) Bright field (BF) TEM image of BCN-graphene; scale bar is 100 nm. d) Atomic-resolution TEM image of BCN-graphene; inset shows a fast-Fourier transform (FFT) pattern.

conditions for the synthesis of BC-graphene and BCN-graphene is the absence or presence of nitrogen.

The morphologies of C-, BC-, and BCN-graphene appear similar to each other in both scanning electron microscope (SEM) and transmission electron microscope (TEM) images (Supporting Information, Figures S2, S3, and S4), and those of BCN-graphene at low magnification show a crumpled and wrinkled sheet structure (Figure 1 b,c; see also Figure S4). At higher magnification (Figure 1 d; see also Figure S4 b), BCN-graphene displayed a strong fast-Fourier transformed (FFT) pattern, which suggests a highly crystalline structure (Figure 1 d, insets; see also Figure S4 b).

The X-ray photoelectron spectroscopy (XPS) spectrum of C-graphene shows C 1s and O 1 s peaks at 284 and 533 eV, along with a weak Cl 2p peak at 198 eV (Figure 2 a and Table S1). There is no detectable N 1s peak in C-graphene, implying that nitrogen was inert to carbon radicals during the reaction. The XPS survey spectrum of BC-graphene is almost identical to that of C-graphene, with no detectable B 1s peak (0.0 at.%). Although incorporation of boron into BC-graphene was detected by time-of-flight secondary-ion mass spectrometry (TOF-SIMS; Figure 2 b), the results indicate that the introduction of boron or nitrogen into the graphitic structure is extremely difficult in the presence of only BBr_3 or nitrogen. However, BCN-graphene, which was prepared in the presence of both BBr_3 and nitrogen, exhibits B 1s (2.38 atom%) and N 1s (2.66 atom%) peaks centered at 190 and 398 eV in the XPS spectra, as well as strong B and N peaks in the TOF-SIMS spectra (Figure 2 a,b). By using the high-resolution B 1s peak, the ratio of B–C/B–N was determined to be approximately 2:1 (Figure 2 a, inset), which matches with the structural unit proposed in Figure S1 d. Furthermore, electron energy-loss spectroscopy (EELS) roughly provided bonding-state information, as heteroatoms (B and N K-edges) and carbon (C K-edge) are connected with an sp^2 hybridized structure (Figure 2 c). EELS shows that each atomic bonding consists of 1s-π* and 1s-σ* bonding, as observed in the XPS spectrum (Figure 2 a, inset). Specifically, the EELS spectrum of BCN-graphene exhibits clear boron, carbon, and nitrogen peaks at 190, 284, and 399 eV, whereas BC-graphene shows a marginally detectable B K-edge (pink circle, Figure 2 c). All elements have both π* and σ* bonding, and are therefore sp^2 hybridized.[27] The distribution of boron, carbon, and nitrogen in the BCN-graphene sheet was mapped using EELS

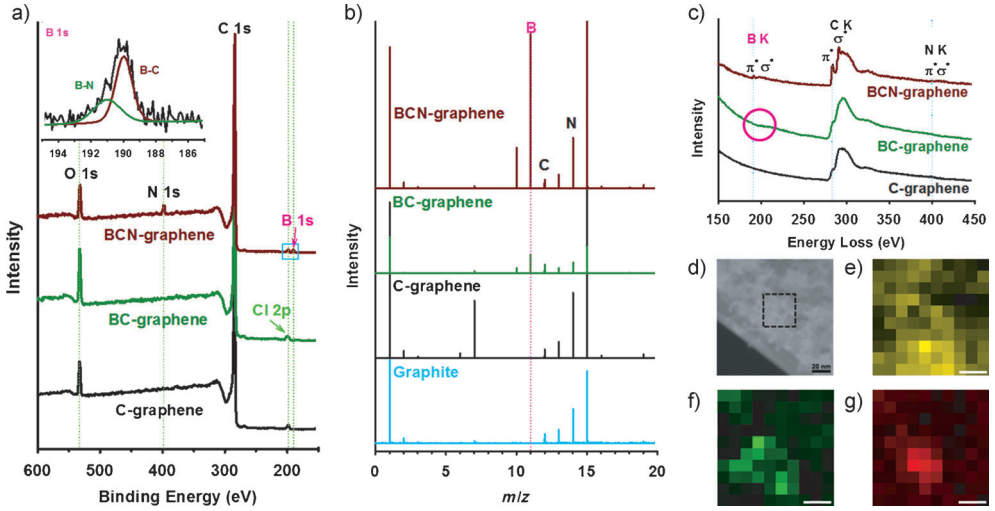

Figure 2. a) XPS survey spectra of samples; inset shows a high-resolution B 1s spectrum of BCN-graphene, marked by a blue square in (a). b) TOF-SIMS spectra; the nitrogen and oxygen peaks were observed in all samples due to chemically/physically attached nitrogen and oxygen. The spectrum from pristine graphite is provided as reference. c) K-shell excitation of boron, carbon, and nitrogen from EELS spectra of samples. d) Dark-field TEM image, dotted region is elemental-map region with 20 nm scale bars; e–g) elemental maps of BCN-graphene: e) carbon; f) boron; g) nitrogen.

elemental mapping (Figure 2d–g). It shows that the boron and nitrogen are co-doped in the BCN-graphene sheet. Acid–base interaction between B and N-containing substrates should be a plausible mechanism for B/N co-doping into the graphitic structure.[28] The proposed mechanism is that BBr_3 interacts with the nitrogen gas first and is then activated by the potassium to generate boron radicals, which subsequently react with carbon radicals to self-assemble into a graphitic structure (Figure S1d). To support the experimental observation of efficient B/N co-doping in BCN-graphene, density functional theory (DFT) calculations were conducted and revealed that the formation energy and crystal lattice energy of the BCN-unit is the lowest among the possible unit reactions (Figure S5). Hence, for the co-doping of boron and nitrogen into a graphitic framework, it is believed that there must be a synergistic contribution to the reaction. Similar to the stable borane–ammonia complex ($H_3B{-}NH_3$),[29] a possible scenario would be the acid–base interaction between BBr_3 (Lewis acid) and nitrogen (Lewis base) to yield a Br_3B-N≡N-BBr_3 intermediate complex (Figure S1), because BBr_3 has the highest Lewis acidity among boron trihalides (BX_3, X = F, Cl, Br). The formation of this complex in situ could promote effective B–N bond formation in the reaction system, which efficiently forms BCN-graphene.

To further investigate the structure of the BCN-graphene, Raman spectra were obtained from all powder samples (Figure S6a).[30] The normalized spectra of all samples display D and G bands at 1343 and 1580 cm^{-1}, respectively, which are associated with the degree of disorder and graphitic symmetry. In all cases, 2D peaks, which are related to the number of graphene sheets, are located at 2680 cm^{-1}. In the cases of C-, BC-, and BCN-graphene, the I_D/I_G ratios are 0.95, 0.92, and 0.70 in that order, indicating that the defect ratios are generally higher than graphene produced from CVD process.[31] The I_{2D}/I_G ratio is 1.35, which implies that C-graphene consists of few layers, even in a powder form. On the other hand, BC- and BCN-graphene have I_{2D}/I_G ratios of 0.67 and 0.62, indicating that they are composed of multilayers.

Thermogravimetric analysis (TGA) suggests that all samples are thermo-oxidatively stable up to 500 °C in air, which indicates that the graphitic networks have well-ordered structures (Figure S6b). X-ray diffraction (XRD) patterns show that the peaks (interlayer d spacing) are located at 26.01° (3.42 Å) for C-graphene, 25.88° (3.44 Å) for BC-graphene and, 25.94° (3.43 Å) for BCN-graphene, respectively (Figure S6c and S6d), all of which are lower (larger d spacing) than the 26.54° (3.34 Å) for pristine graphite.[32] Furthermore, the relative peak intensities of (002) of C-, BC-, and BCN-graphene were 0.72, 0.30, and 0.48 % of that of pristine graphite, thus indicating that solvothermally synthesized graphene stays in crumpled and wrinkled forms (Figure 1b,c, S2–S4). As a result, efficient stacking is limited, unlike pristine graphite, which forms large number of stacked layers.

The specific surface area, as determined by nitrogen adsorption-desorption isotherms, also increases in the order of C-graphene (109.2 $m^2 g^{-1}$), BC-graphene (171.9 $m^2 g^{-1}$), and BCN-graphene (201.5 $m^2 g^{-1}$; Figure S7 and Table S2). The values are well-correlated with the degree of crumples/wrinkles in the samples, which depends upon the doping states. It is supposed that doped heteroatoms in the graphitic carbon framework create not only a crumpled/wrinkled morphology, but also provide active sites for efficient gas absorption by charge polarization. More interestingly, the dispersion stability of BCN-graphene in *N*-methyl-2-pyrrolidone (NMP; Figure S8 and Table S3), which is the most crumpled/wrinkled and with highest surface area, is the best among the samples. BCN-graphene remains stable for two months, allowing easy fabrication of thin films, and thus has a broad application potential.

As an example, FET devices were fabricated with BCN-graphene as the active layer (Figure 3a, inset), which was dispersed in NMP and cast as a thin film on a SiO_2 (300 nm)/Si substrate with a thickness of approximately 4 nm (Figure 3b).

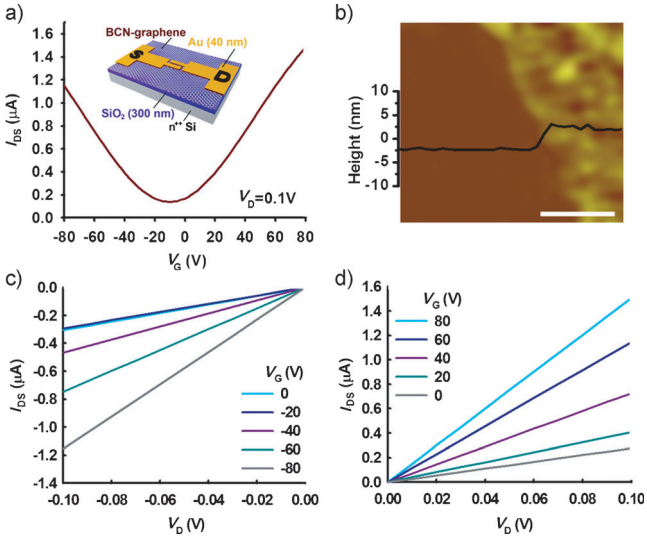

Figure 3. a) The transfer curve of BCN-graphene FET at a drain voltage of 0.1 V; inset shows an illustration of BCN-graphene FET. b) Tapping-mode AFM image of BCN-graphene film on a SiO_2/Si wafer; the embedded graph is the thickness profile, the scale bar is 200 nm. c,d) Output curves of BCN-graphene FET at different gate voltages: c) *p*-type output curves, d) n-type output curves.

The channel width-to-length ratio (W/L) of the FETs is 10, with $L = 500$ nm. A typical transfer curve of BCN-graphene is displayed in Figure 3a. The hole and electron mobilities were calculated from the linear regime of the transfer characteristics according to the equation:

$$I_D = \mu \frac{W}{L} C_i V_D (V_G - V_{th})$$

where I_D is the drain current, μ is the field-effect mobility, C_i is the specific capacitance of the dielectric, V_D is the drain voltage, V_G is the gate voltage, V_{th} is the threshold voltage. Hole and electron mobilities from the transfer curve (V_D = 0.1 V) in Figure 3a were 2.0 and 2.1 $cm^2 V^{-1} s^{-1}$, respectively, and the average electrical properties are summarized in Table S4. The output curves show ambipolar characteristics (Figure 3c,d). The low hole and electron mobilities resulted

from the scattering at the junction by the stacking of individual BCN-graphene flake sheets. It was expected that by co-doping boron and nitrogen into the basal plane of graphene, the band-gap would increase, but the Dirac point would stay near 0 V because of charge neutralization between boron and nitrogen. However, in the case of BCN-graphene, the Dirac point was located at −10 V, and thus an n-type behavior, owing to the slightly higher amount of nitrogen (2.66 atom%) as well as a much stronger electronegativity ($\chi = 3.04$) than those of boron (2.38 atom% and $\chi = 2.04$, respectively; Table S1). The on/off current ratio was 10.7, which shows that BCN-graphene behaves as a semiconductor. In addition, the optical band gap is about 3.3 eV (Figure S9), further confirming the semiconducting behavior. Although graphene-oxide and doped-graphene-oxide films are easy to fabricate, it is difficult to use as an n-type semiconductor with an open band gap.[33–36] BCN-graphene overcomes this difficulty while maintaining easy processability, which could offer many more practical applications.

In summary, a new method for the synthesis of boron/nitrogen co-doped graphene (BCN-graphene) was created. Boron tribromide as a boron feedstock and nitrogen gas as a nitrogen feedstock have a synergistic effect for boron and nitrogen co-doping into the graphitic network when they are applied together with CCl_4. On the other hand, the reaction of CCl_4 with either boron tribromide or nitrogen gas alone leads to a marginal or zero doping level. The dispersion stability of BCN-graphene was also improved by co-doping, leading to enhanced processability. Thus, BCN-graphene allowed the fabrication of a FET device by solution casting. The device demonstrated a 10.7 on/off ratio and semiconducting nature with optical band-gap of 3.3 eV. Combined with scalable production and the high dispersion stability, the BCN-graphene shows high potential for many practical applications.

Received: November 26, 2013

Keywords: boron · doping · field effect transistors · graphene · nitrogen

[1] K. S. Novoselov, A. K. Geim, S. V. Morozov, D. Jiang, Y. Zhang, S. V. Dubonos, I. V. Grigorieva, A. A. Firsov, *Science* **2004**, *306*, 666 – 669.
[2] A. Peigney, C. Laurent, E. Flahaut, R. Bacsa, A. Rousset, *Carbon* **2001**, *39*, 507 – 514.
[3] A. A. Balandin, S. Ghosh, W. Bao, I. Calizo, D. Teweldebrhan, F. Miao, C. N. Lau, *Nano Lett.* **2008**, *8*, 902 – 907.
[4] K. I. Bolotin, K. Sikes, Z. Jiang, M. Klima, G. Fudenberg, J. Hone, P. Kim, H. Stormer, *Solid State Commun.* **2008**, *146*, 351 – 355.
[5] R. Nair, P. Blake, A. Grigorenko, K. Novoselov, T. Booth, T. Stauber, N. Peres, A. Geim, *Science* **2008**, *320*, 1308 – 1308.
[6] F. Bonaccorso, Z. Sun, T. Hasan, A. Ferrari, *Nat. Photonics* **2010**, *4*, 611 – 622.
[7] C. Lee, X. Wei, J. W. Kysar, J. Hone, *Science* **2008**, *321*, 385 – 388.
[8] H. Wang, T. Maiyalagan, X. Wang, *ACS Catal.* **2012**, *2*, 781 – 794.
[9] F. Schedin, A. Geim, S. Morozov, E. Hill, P. Blake, M. Katsnelson, K. Novoselov, *Nat. Mater.* **2007**, *6*, 652 – 655.
[10] A. Varykhalov, M. R. Scholz, T. K. Kim, O. Rader, *Phys. Rev. B* **2010**, *82*, 121101.
[11] Y. Liang, Y. Li, H. Wang, J. Zhou, J. Wang, T. Regier, H. Dai, *Nat. Mater.* **2011**, *10*, 780 – 786.
[12] J. M. Englert, C. Dotzer, G. Yang, M. Schmid, C. Papp, J. M. Gottfried, H.-P. Steinrück, E. Spiecker, F. Hauke, A. Hirsch, *Nat. Chem.* **2011**, *3*, 279 – 286.
[13] Y. Sun, Q. Wu, G. Shi, *Energy Environ. Sci.* **2011**, *4*, 1113 – 1132.
[14] H.-J. Choi, S.-M. Jung, J.-M. Seo, D. W. Chang, L. Dai, J.-B. Baek, *Nano Energy* **2012**, *1*, 534 – 551.
[15] X. Wang, X. Li, L. Zhang, Y. Yoon, P. K. Weber, H. Wang, J. Guo, H. Dai, *Science* **2009**, *324*, 768 – 771.
[16] Z. Sun, D. K. James, J. M. Tour, *J. Phys. Chem. Lett.* **2011**, *2*, 2425 – 2432.
[17] A. K. Geim, K. S. Novoselov, *Nat. Mater.* **2007**, *6*, 183 – 191.
[18] D. Wei, Y. Liu, Y. Wang, H. Zhang, L. Huang, G. Yu, *Nano Lett.* **2009**, *9*, 1752 – 1758.
[19] X. Li, X. Wang, L. Zhang, S. Lee, H. Dai, *Science* **2008**, *319*, 1229 – 1232.
[20] L. Britnell, R. V. Gorbachev, R. Jalil, B. D. Belle, F. Schedin, A. Mishchenko, T. Georgiou, M. I. Katsnelson, L. Eaves, S. V. Morozov, N. M. R. Peres, J. Leist, A. K. Geim, K. S. Novoselov, L. A. Ponomarenko, *Science* **2012**, *335*, 947 – 950.
[21] J. Lu, K. Zhang, X. F. Liu, H. Zhang, T. C. Sum, A. H. Castro Neto, K. P. Loh, *Nat. Commun.* **2013**, *4*, 2861.
[22] Z. Xu, W. Lu, W. Wang, C. Gu, K. Liu, X. Bai, E. Wang, H. Dai, *Adv. Mater.* **2008**, *20*, 3615 – 3619.
[23] C.-K. Chang, S. Kataria, C.-C. Kuo, A. Ganguly, B.-Y. Wang, J.-Y. Hwang, K.-J. Huang, W.-H. Yang, S.-B. Wang, C.-H. Chuang, M. Chen, C.-I. Huang, W.-F. Pong, K.-J. Song, S.-J. Chang, J.-H. Guo, Y. Tai, M. Tsujimoto, S. Isoda, C.-W. Chen, L.-C. Chen, K.-H. Chen, *ACS Nano* **2013**, *7*, 1333 – 1341.
[24] T. Lin, F. Huang, J. Liang, Y. Wang, *Energy Environ. Sci.* **2011**, *4*, 862 – 865.
[25] M. Choucair, P. Thordarson, J. A. Stride, *Nat. Nanotechnol.* **2008**, *3*, 30 – 33.
[26] X. Lü, J. Wu, T. Lin, D. Wan, F. Huang, X. Xie, M. Jiang, *J. Mater. Chem.* **2011**, *21*, 10685 – 10689.
[27] L. Ci, L. Song, C. Jin, D. Jariwala, D. Wu, Y. Li, A. Srivastava, Z. Wang, K. Storr, L. Balicas, *Nat. Mater.* **2010**, *9*, 430 – 435.
[28] K. Niedenzu, J. W. Dawson, *J. Am. Chem. Soc.* **1960**, *82*, 4223 – 4228.
[29] S. G. Shore, K. W. Boddeker, *Inorg. Chem.* **1964**, *3*, 914 – 915.
[30] A. Ferrari, J. Meyer, V. Scardaci, C. Casiraghi, M. Lazzeri, F. Mauri, S. Piscanec, D. Jiang, K. Novoselov, S. Roth, *Phys. Rev. Lett.* **2006**, *97*, 187401.
[31] S. Bae, H. Kim, Y. Lee, X. Xu, J.-S. Park, Y. Zheng, J. Balakrishnan, T. Lei, H. R. Kim, Y. I. Song, Y.-J. Kim, K. S. Kim, B. Ozyilmaz, J.-H. Ahn, B. H. Hong, S. Iijima, *Nat. Nanotechnol.* **2010**, *5*, 574 – 578.
[32] I.-Y. Jeon, H.-J. Choi, M. J. Ju, I. T. Choi, K. Lim, J. Ko, H. K. Kim, J. C. Kim, J.-J. Lee, D. Shin, S.-M. Jung, J.-M. Seo, M.-J. Kim, N. Park, L. Dai, J.-B. Baek, *Sci. Rep.* **2013**, *3*, 2260.
[33] G. Eda, G. Fanchini, M. Chhowalla, *Nat. Nanotechnol.* **2008**, *3*, 270 – 274.
[34] D. W. Chang, E. K. Lee, E. Y. Park, H. Yu, H.-J. Choi, I.-Y. Jeon, G.-J. Sohn, D. Shin, N. Park, J. H. Oh, L. Dai, J.-B. Baek, *J. Am. Chem. Soc.* **2013**, *135*, 8981 – 8988.
[35] Q. He, S. Wu, S. Gao, X. Cao, Z. Yin, H. Li, P. Chen, H. Zhang, *ACS Nano* **2011**, *5*, 5038 – 5044.
[36] S.-K. Lee, H. Y. Jang, S. Jang, E. Choi, B. H. Hong, J. Lee, S. Park, J.-H. Ahn, *Nano Lett.* **2012**, *12*, 3472 – 3476.

